Optica Applicata, Vol. XXI, No. 1, 1991

Variable wavelength interferometry. IX Accuracy

MAKSYMILIAN PLUTA

Central Optical Laboratory, ul. Kamionkowska 18, 03-805 Warszawa, Poland.

A versatile interferometric method has been developed and described in a number of papers of this series. The method is based on the use of monochromatic light whose wavelength is continuously varied (decreased) to bring into coincident and/or anticoincident configurations of displaced and undisplaced interference fringes (VAWI–1 technique). Another version of this method uses two pointer lines whose distance is equal to about ten interfringe spacings in the red region of the visible spectrum (VAWI–2 technique). One of these lines is permanently brought into coincidence with the centre of the zero-order interference fringe of the empty interference field, while the consecutive high-order fringes, undisplaced and then displaced, are brought into coincidence with the other line when the wavelength of the monochromatic light is varied. An intermediate version of the variable wavelength interferometric (VAWI) method between VAWI–1 and VAWI–2 technique uses a single pointer line and is referred to as the VAWI–3 technique. All these techniques, their principles and applications, have been described in the preceding papers of this series with special emphasis put on their combination with double-refracting microinterferometry. Now, the accuracies of these techniques will be discussed in more detail.

1. Introduction

Possible errors or uncertainties of the VAWI method and its specific techniques, VAWI–1 to VAWI–3, like those of conventional interferometry, can be divided into four categories:

i) Instrumental errors. These are caused by possible optical and mechanical defects of the interferometer used. The insufficient degree of light monochromacy can also be qualifited among error sources of this category.

ii) Reading errors. These occur because the operator is not perfect in reading the scale of a device by means of which the interfringe spacings b are measured. A characteristic feature of the VAWI method lies in the fact that the only parameters to be directly measured are the interfringe spacings, while other interferometric quantities are observed, read from the calibration graph $b(\lambda)$, and derived from quite simple formulae. If the relationship between b and the light wavelength λ is well defined (as, in fact, it was in the VAWI techniques discussed up to now), the plot $b(\lambda)$ is considered as the basic calibration graph. If the calibration procedure was carried out very carefully, once plotted $b(\lambda)$ graph is permanently valid. However, some errors can also occur when the wavelengths λ are read from this graph. In the case of on-line processing of fringe interference patterns with the help of an electronic processor and computer, this category of subjective errors does not occur.

iii) Specimen errors. These arise beacuse of possible variations in the object

under study. In particular, liquid objects can suffer from changes of their refractive index due to temperature variations. These sources of errors will be ignored here. More serious error sources, however, lie in the spectral dispersion of refractive index or that of birefringence if the optical properties of a specimen to be measured are far from the specific situations referred to as object-adapted variable-wavelength interferometry [1], [2].

iv) Repeatability errors. These errors arise whenever a module or component of the interferometric system has been re-set between successive measurements or the system has been re-adjusted.

The accuracy of the VAWI method within the scope of the error sources mentioned above will be discussed below. As previously in the papers of this series, the double-refracting microinterferometer (see Fig. 2 in [3]) is taken into account. That interference system is especially suitable for the VAWI method, due to its well defined relationship between the light wavelength λ and the interfringe spacing b; moreover, its spectral dispersion properties (birefringence of quartz crystals of which the double-refracting prisms are made) are exactly known. Additionally, the system in question is free from defects (or errors) of both optical and mechanical instabilities.

2. Variable interfringe spacing across the image plane

Double-refracting microinterferometers based on the Wollaston prism suffer from a slightly variable interfringe spacing b' across the image plane Π' (Fig. 1), though the Wollaston prism itself produces its own fringe pattern with a constant interfringe spacing b across the plane of localization of interference fringes PLI. The spacing b is given by a well known formula

$$b = \frac{\lambda}{\varepsilon} = \frac{\lambda}{2(n_e - n_o)\tan\alpha} = \frac{\lambda}{2D\tan\alpha} \tag{1}$$

where λ is the light wavelength, ε is the angular wavefront shear produced by the Wollaston prism W_2 and expressed in radions, $n_e - n_o = D$ is the birefringence of a crystal of which the prism W_2 is made, and α is the apex angle of this prism. On the other hand, the interfringe spacing b' in the image plane Π' is given by

$$b' = \frac{h}{g} b \tag{2}$$

Fig. 1. Double-refracting microinterferometric system applied to the VAWI method. WIF – wedge interference filter (linear variable interference filter VERIL S 200), P – polarizer, D – slit dipahragm, C – condenser, F_c – its front focal point, Π – object plane, O – object, Ob – objective, F' – its back focal point, W_0 – objective birefringent prism of the Nomarski type, W_2 – tube birefringent (Wollaston) prism and its own interference fringes (to the right) localized in the plane PLI, PS – micrometric screw for transverse sliding the prism W_2 and thus for measurement of the interfringe spacing b, A – analyser, Π' – image plane and interference fringes (to the right) observed through the ocular Oc whose front focal F_{oc} is coincident with Π', FP – focal plate with a pointer line PL. To the right of the condenser, the Wollaston prism W_2 seen from above, the transmission axes PP and AA of the polarizer P and analyser A, and the

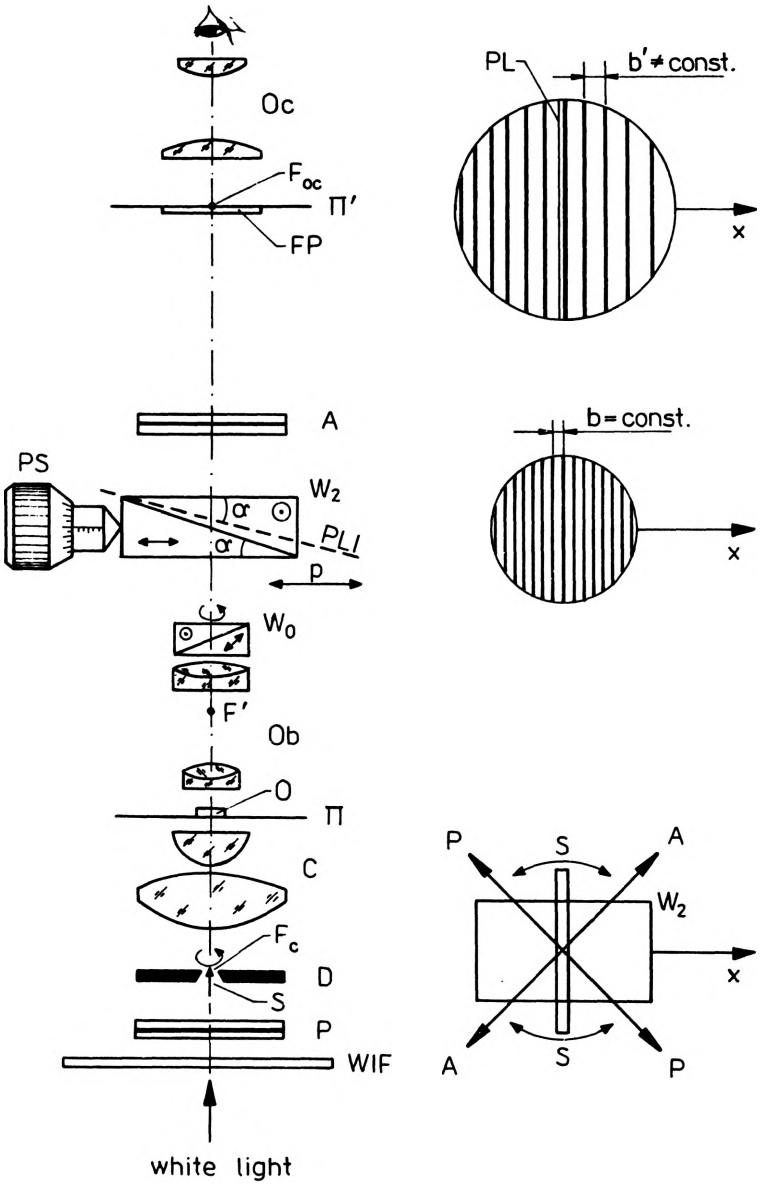

slit S of the diaphragm D are shown. The prism W_0 and slit S can be rotated about the optical axis of the microinterferometric system to orientate this prism in four priviledged positions (additive, subtractive, crossed, and neutral) with respect to the prism W_2; respectively, the slit S is always oriented at right angles to the direction of the resultant wavefront shear produced by the prisms W_0 and W_2. The plane of localization of own interference fringes of the prism W_0 is coincident with the objective focal point F', and thus this prism does not produce any fringes in the image plane Π'; only the prism W_2 is responsible for the interference fringes in this plane as shown to the right

where h is the optical tube length of the microscope objective Ob, and g is the distance between the objective focal plane F′ and the plane PLI (derivation of Eq. (2) can be found in [4]). The latter is not perpendicular to the objective axis but slanted at an angle equal approximately to 0.65α [4]. Consequently, the distance g is different for interference fringes of different orders, and thus Eq. (2) shows that the interfringe spacing b' increases systematically from the left-hand side to the right-hand side of the image plane Π'. The variation $\Delta b'$ can be expressed as (see [4])

$$\Delta b' = b'_m - b'_{m-1} = \frac{bh}{g_o^2}\Delta g \tag{3}$$

where the subscript m denotes the order of interference fringes, g_o is the distance g along the optical axis of the microscope objective Ob, and $\Delta g = g_m - g_{m-1}$.

In practice, the optical path difference δ produced by an object under study is frequently determined from the formula

$$\delta = \frac{c'}{\overline{b'}}\lambda \tag{4}$$

where c' is the interference fringe displacement caused by the object in the image plane Π'. The quantities being measured directly are b' and c'. The displacement c' must, of course, be measured between interference fringes belonging to the same interference order, say, to the zero order. No problem arises if the interfringe spacing b' in the image plane Π' is a constant parameter along a coordinate x perpendicular to the straight-line fringes in this plane. Otherwise, if b' is a spatially variable parameter, the optical path difference cannot exactly be determined, especially when $c' > b'$. A possible error $\Delta\delta$ in the measurement of δ is given by the following formula [4]:

$$\Delta\delta = (\Delta b')_N \delta \tag{5}$$

where

$$(\Delta b')_N = \frac{\Delta b'}{\overline{b'}} = \frac{B'_{2m}}{2m}. \tag{6}$$

Here $\overline{b'}$ is the mean interfringe spacing which can be measured in the image plane Π', and B'_{2m} is the distance between the interference fringes of $-m$ and $+m$ orders as shown in Fig. 1.

The above instrumental error does not occur if the optical path difference δ is measured by transverse sliding the Wollaston prism W_2 in the direction marked by the arrow p in Fig. 1. The transverse translation introduces a continuously variable optical path difference Δ (or phase shift $\psi = 2\pi\Delta/\lambda$) between sheared wavefronts and the interference fringes move in the same direction p across the field of view. A micrometer drive screw PS, by means of which the prism is slid, can therefore be referred to as the phase screw. The relationship between Δ and the transverse displacement of the prism W_2 is linear (see Fig. 4 in [5]). This fact allows the

optical path difference δ produced by an object under study O to be measured by using the lateral translation of the Wollaston prism, which now functions simultaneously as a wavefront shear device and a measuring phase compensator. Such a double function of the Wollaston prism was originally applied in practice by the author of this paper more than thirty years ago [6] and standardly introduced to the double-refracting microinterferometer in question.

When the interference fringe of zero order is exactly coincident with a pointer line (PL) of the ocular Oc (Fig. 1), the position of the Wollaston prism W_2 will be referred to as the zero position p_0. The transverse movement of this prism, starting from p_0, causes the fringes of consecutive interference orders to be brought into coincidence with the ocular pointer line PL. If the consecutive coincidence positions p_{+1}, p_{+2}, p_{+3},... (for interference fringes of positive orders) or p_{-1}, p_{-2}, p_{-3},... (for fringes of negative interference orders) are read on the scale of the phase screw PS, the differences $p_{+1}-p_0$, $p_{+2}-p_{+1}$, $p_{+3}-p_{-2}$,... or $p_{-1}-p_0$, $p_{-2}-p_{-1}$, $p_{-3}-p_{-2}$,... correspond to the interfringe spacing b defined by Eq. (1). The relation between p_m-p_0 and mb (here $m = \pm 1, \pm 2, \pm 3,...$) is strictly linear (see Fig. 4 in [5], as mentioned above). It is self-evident that the translation of the Wollaston prism by b, $2b$, $3b$,... cause the optical path difference Δ between interfering wavefronts to be changed by λ, 2λ, 3λ,....

The transverse translation of the Wollaston prism enables a quantity c equivalent to the fringe displacement c', introduced by the object under study (O, Fig. 1) to the interference field observed through the ocular Oc, to be determined as well. To achieve this the Wollaston prism W is displaced to such a particular position p_c, for which the displaced fringe of the zero interference order (or that of another known order m) is brought into coincidence with the ocular pointer line PL. The difference $p_c-p_0 = c$ (or $p_c-p_m = c$) read on the scale of the phase screw PS corresponds to the fringe displacement c' occurring in the image plane Π'. Consequently Eq. (4) may now be rewritten as

$$\delta = \frac{c}{b}\lambda. \tag{7}$$

The above procedure refers to conventional microinterferometry using the double-refracting system shown in Fig. 1 (see also Fig. 2 in [2]). Another situation occurs if the VAWI–1 technique is used. This technique is based on the use monochromatic light whose wavelength is continuously decreased to bring into coincident and/or anticoincident configurations of displaced and undisplaced interference fringes in the image plane, and on the simultaneous mesurement of the interfinge spacings $b_s = b_1, b_2, b_3,...$ corresponding to light wavelengths $\lambda_s = \lambda_1, \lambda_2, \lambda_3,...$ which produce the above mentioned configurations of interference fringes. Let the coincident configurations be taken into account, and the transparent object (O, Fig. 1) is assumed to be an elongated strip of uniform optical thickness. The strip is oriented at right angles to the interference fringes and its images O′ and O″ (Fig. 2) are totally sheared when the objective birefringent prism W_0 is crossed with the tube Wollaston prism W_2. For particular light wavelengths λ_s mentioned above, the fringes displaced

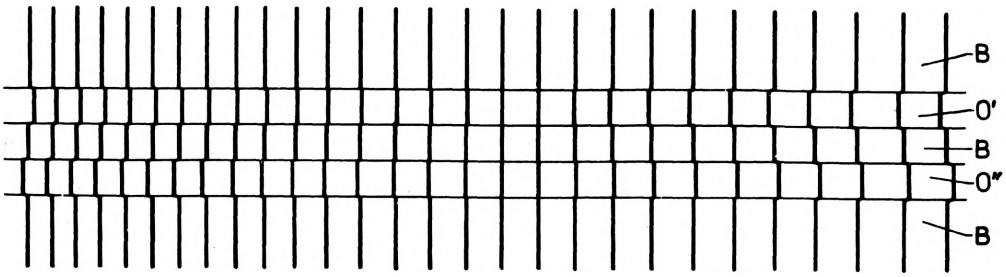

Fig. 2. Defect of a coincident configuration of interference fringes, due to the slightly variable interfringe spacing (b') across the image plane (Π') of the microinterferometric system shown in Fig. 1. B – background and fringes of the empty interference field, O' and O'' – fully sheared images of an extended and uniform strip object, and interference fringes displaced (in oposite directions) by this object by several interfringe spacings and then brought into coincidence with the undisplaced fringe of the empty interference field. The fringe coincidence(s) is (are) achieved by varying the light wavelength using the wedge interference filter (WIF, Fig. 1)

by the object become coincident with those of the background (B). Due to the variable interfringe spacing across the image field, discussed above, an ideal coincidence, such as shown in the centre of Fig. 2, can be obtained only for a limited number of interference fringes, whereas the other fringes form slightly decoincident configurations (the figure is not true to scale; in fact, the interfringe spacing inconstancy and fringe decoincidences are much smaller). This defect, however, does not lead to the accuracy degradation of the VAWI–1 technique if a local optical path difference δ is measured on an object region, where an excellent fringe coincidence occurs (see the centre region of Fig. 2). The same statement holds for the VAWI–3 technique.

On the other hand, the interfringe spacing inconstancy degrades the accuracy of the VAWI–2 technique [7], [8]. For this technique a gauging graticule, consisting of two pointer lines L_1 and L_2, is used (see Figs. 1 and 2 in [8]). The distance between these lines is selected to be as along as possible, say, equal to $10b_1$. One line is permanently brought into coincidence with the centre of zero-order fringe of the empty interference field, while the consecutive high-order fringes, undisplaced and then displaced, are brought into coinidence with the other pointer line, when the wavelength of the monochromatic light is decreased. Due to the inconstancy of the interfringe spacing in the image plane, the results obtained for the optical path difference δ can be slightly either higher or lower than the true value of δ. If, however, the roles of the pointer lines L_1 and L_2 are replaced and we perform two measuring processes on the same object region, then we obtain two results the mean of which represents the true value of δ much more accurately.

In order cancel the variable interfringe spacing in the image plane, the so-called symmetrical Wollaston prism (Fig. 3**a**) must be used. Its plane of localization of interference fringes (PLI) is parallel to the external faces of the prism and lies between these faces at a distance equal to half of the prism thickness. If this prism is adjusted at right angles to the optical axis of the microscope objective Ob (Fig. 1),

the plane PLI is also perpendicular to this axis, and thus a constant intefringe spacing b' occurs in the image plane Π' of the microinterferometer in question.

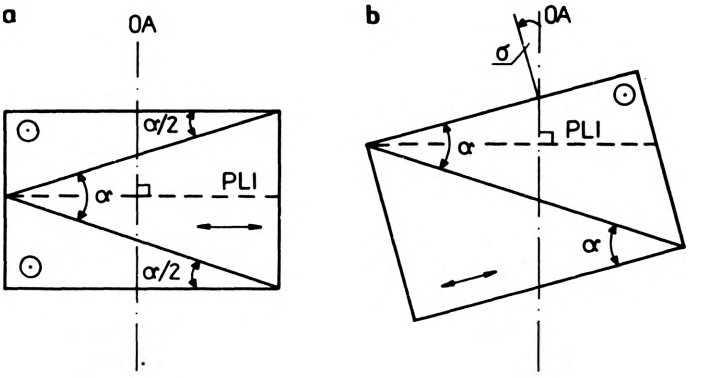

Fig. 3. Symmetric (**a**) and typical (**b**) Wollaston prisms adjusted to such a position that their planes of localization (PLI) of their own interference fringes are exactly at right angles to the optical axis OA of the microscope objective (Ob, Fig. 1)

It is also worthwhile nothing that the uniform distribution of interference fringes in the image plane may also be achieved with a typical Wollaston prism (Fig. 3**b**), if this is slanted so that its plane of localization of interference fringes becomes perpendicular to the optical axis of the microinterferometer. However, this possibility may only be recommended when the apex angle α of the Wollaston prism is small, say, not greater than 5°.

On the other hand, a slanted Wollaston prism is useful for reflected-light microinterferometry whose performance is reduced by stray light generated by reflections of illuminating rays at the surface of optical elements (see [9]). Unwanted reflections are produced, in particular, by the plane surfaces of the Wollaston prism. To overcome this defect, the prism is usually not placed at right angles to the objective axis (OA, Fig. 3), but is slightly slanted. The slant angle σ is adjusted so as to reject reflections outside the field of view of the microinterferometer and to make the plane PLI as perpendicular as possible to the objective axis OA. This is possible if the apex angle α of the Wollaston prism is not greater than 5° as mentioned above.

3. Degree of light monochromacity

It is self-evident that the VAWI method and all its specific versions function more and more accurately if the light used is more and more monochromatic. At any rate, the primary calibration $b(\lambda)$ must be performed by using extremely monochromatic light, say, laser light sources (see [3] and [10]). These enable a calibration accuracy: $\Delta b/b = 0.005\%$ and $\Delta\lambda/\lambda = 0.005\%$ to be obtained.

Due to the slit diaphragm (D, Fig. 1), the microinterferometer in question co-operates well with a continuous wavelength interference monochromator (wedge

interference filter) WIF. This component of the VAWI instrumentation is located as near as possible to the above mentioned diaphragm, whose slit (S) is normally not larger than 0.5 mm. A tungsten-halogen light source (12 V/100 W) is standardly recommended, from which monochromatic light of continuously variable wavelength is extracted by transverse sliding the filter WIF.

The VERIL S 200 filter has appeared to be suitable well for the VAWI method. The basic parameters of this wedge interference filter are listed in Table 1 (after technical catalogue of the manufacturer, the Schott Glaswerke, Mainz, Germany). Its local spectral transmission curves are similar to those of high quality homogenous

Table 1. Basic parameters of the linear variable interference filter VERIL S 200 (Schott Glaswerke, Mainz)

Length in mm	200 +0 −0.3
Width in mm	25 +0 −0.3
Thickness in mm	max. 6
Spectral range in nm	400–700
Length of spectrum in mm	111–142
Dispersion in mm/nm	0.37–0.47
Half bandwidth in nm for wavelengths:	
450 nm	10–16
550 nm	10–14
650 nm	10–18
Maximum transmittance for wavelengths:	
450 nm	$\geqslant 0.25$
550 nm	$\geqslant 0.30$
650 nm	$\geqslant 0.25$
Tenth bandwidth in nm	18–32
Thousandth bandwidth in nm	70–125
Blocking range in nm	up to 750
Maximum transmittance in blocking range	10^{-3}

interference filters [3], and its peak wavelength changes gradually over the length of the filter strip. The undesirable secondary transmission spectrum is blocked by a graduated colour glass. When such a filter is used with a slit diaphragm, broadening the slit leads to a wider transmission curve and reduction of the maximum transmittance τ_{max} (see Table 1). In the VERIL S 200, slit widths of up to 3 mm have practically no influence on the general fitering effect; the peak wavelength, however, changes according to the filter dispersion as specified in Table 1 (0.37–0.47 mm/nm). A special manufacturing method of these interference filters leads to slight deviations in the spectral dispersion from filter to filter. This defect, however, has no importance in the VAWI techniques, due to the fact that the local peak wavelength λ of this filter is determined in real time by measuring the interfringe spacing b and then using the calibration plot $b(\lambda)$, whose accuracy is much better than the filter spectral dispersion mentioned above.

4. Accuracy of the measurement of interfringe spacing

One of the most important featuress of the VAWI method is the fact that the interfringe spacings are only directly measured, while the other parameters and quantities required for the final interferometric results are observed (the interference order increments q_s), calculated from quite simple formulae (the initial interference order m_1), and read out from the calibration graph $b(\lambda)$ plotted once and for all on a graph paper or stored in a microcomputer memory. As mentioned above, the graph $b(\lambda)$ is primarily used for reading the light wavelengths as function of the interfringe spacings directly measured by means of the phase screw PS (Fig. 1). It is, therefore, important to know the possible errors Δb arising in the measurement of the interfringe spacings.

The micrometric phase screw PS (Fig. 1) has a scale whose elementary divisions are equal to 10 μm, but using a loupe permits us to read this scale with an accuracy up to 1μm. Thus, the main source of the errors in measuring the interfringe spacings does not lie in reading the scale of the phase screw, but is rather associated with inaccuracies in coincidings the centre of interference fringes with the pointer line PL of a focal plate of the ocular Oc (Fig. 1). The accurate coincidence may be estimated much better if the pointer line is symmetrically surrounded by two additional lines as shown in Fig. 4. Such an ocular graticule permits us to divide the interference

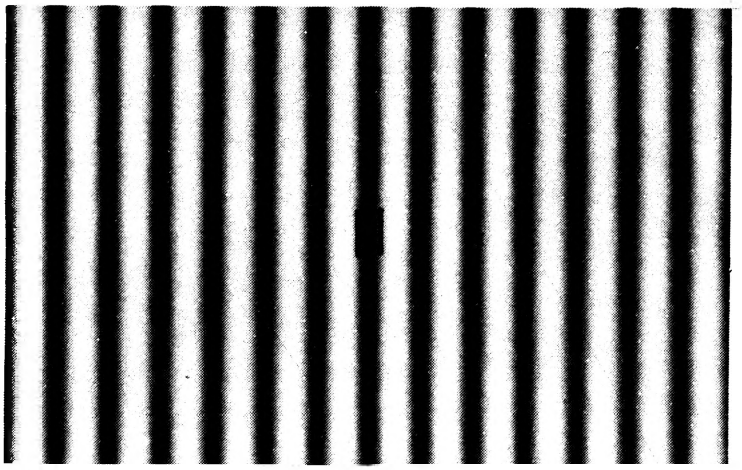

Fig. 4. Fringe interference field and an ocular graticule with a central pointer line PL and two side-lines. The latter enable the centre of interference fringes to be brought into coincidence with the pointer line PL more precisely than without them

fringe into two adjacent areas and is therefore more accurate than that with a single pointer line, as the human eye estimates more precisely the darkness equality of two adjacent areas than the central position of the pointer line with respect to the interference fringe.

A distance l equivalent to multiple interfringe spacings, e.g., $l = 10b$ or $l = 20b$ between interference fringes of plus and minus five or ten orders, respectively, rather than a single interfringe spacing is measured across the empty interference field, leading to more accurate values for b. Measuring accuracy $\Delta l = 2$ μm for $l = 20b$ is easily obtained, thus $\Delta b = 0.1$ μm (the measurement of $l > 30\,b$ is not recommended due to weak contrast of fringes whose orders are higher than plus and minus fifteen, in a moderately monochromatic light produced by the VERIL S 200 filter; this limitation, however, does not apply to highly monochromatic light).

The accuracies achieved for the interfringe spacing measurements in differnt spectral regions have been verified by repeating a number of experiments within a period of several days. The summary results are listed in Table 2. As can be seen, the standard deviations* σ_2, σ_{10} and σ_{20} in the unit attributed to the distances $l_2 = 2b$, $l_{10} = 10b$ and $l_{20} = 20b$ are the same (or increase only slightly); and thus, the standard deviation σ here assumed to be equal to Δb and attributed to b, decreases significantly as the distance l increases. This can even be selected as large as $100b$ when highly monochromatic, say, laser light is used, and Δb as small as 0.01 μm may be obtained. Such a high accuracy is not necessary for most typical interferometric measurements; it, however, is required for the master calibration of the microinterferometer to perform an extremely accurate plot $b(\lambda)$ once and for all.

5. Accuracy of fringe coincidence/anticoincidence

The most powerful version of the VAWI method, the VAWI–1 technique, is based on the use of monochromatic light whose wavelength is decreased across the entire visible spectrum to bring into coincident (see Fig. 5 in [3]) and/or anticoincident configurations of diplaced I' and undisplaced I interference fringes. Such fringe configurations may precisely be fixed since the so-called vernier principle is applicable here. In visual interferometry, this principle functions especially well if the object under study is a plate-like strip or edge and causes no bending of displaced interference fringes as shown in Fig. 2. If, however, the object is non-flat (e.g., a cylindric fibre), it deforms the displaced fringes in a more or less parabolic way and the vernier principle is perturbed. Fortunately, we can additionally use the ocular pointer line PL (Fig. 1) to which the coincident and/or anticoincident positions of displaced and undisplaced interference fringes are adjusted.

Due to the consecutive coincident and anticoincident configurations of the interference fringes we obtain a number of specific light wavelengths $\lambda_s = \lambda_1$, $\lambda_2, < \lambda_1$, $\lambda_3 < \lambda_2, \ldots$, the same number of respective interfringe spacings $b_s = b_1$,

---

* Expressed as

$$\sigma = \sqrt{\frac{1}{M-1} \sum_{i=1}^{M} (x_i - \bar{x})^2}$$

where $\bar{x}$ is the arthmetic mean of the quantity measured M times. Here M was equal to 10.

Table 2. Typical results of the measurement of interfringe spacings b and their standard deviations (rms errors) σ or Δb, expressed in micrometers. Distances $l_2 = 2b$, $l_{10} = 10b$, and $l_{20} = 20b$ were measured between the fringes of ± 1, ± 5, and ± 10 interference orders, respectively, in blue, green, yellow, and red spectral regions

Spectral region	± 1 orders				± 5 orders				± 10 orders				$\bar{b}$ (mean)
	l_2	σ_2 for l_2	b	Δb	l_{10}	σ_{10} for l_{10}	b	Δb	l_{20}	σ_{20} for l_{20}	b	Δb	
blue ($\lambda = 483.2$ nm)	324.5	1.29	162.25	0.65 (0.4%)	1628.4	1.17	162.84	0.12 (0.07%)	3252.3	1.15	162.62	0.06 (0.04%)	162.73
green ($\lambda = 528.9$ nm)	358.9	0.93	179.45	0.46 (0.26%)	1800.1	1.66	180.01	0.17 (0.09%)	3599.4	0.84	179.97	0.04 (0.02%)	179.99
yellow ($\lambda = 586.7$ nm)	403.1	1.00	201.55	0.50 (0.25%)	2016.1	1.59	201.61	0.16 (0.08%)	4038.2	1.69	201.91	0.08 (0.04%)	201.76
red ($\lambda = 626.0$ nm)	432.2	1.09	216.1	0.55 (0.25%)	2162.6	1.90	216.26	0.19 (0.09%)	4330.9	2.13	216.55	0.11 (0.05%)	216.50
mean values of standard deviations		1.0	0.50 (0.3%)			1.58		0.16 (0.08%)		1.45		0.06 (0.04%)	

$b_2 < b_1$, $b_3 < b_2$,... and that of interference order increments $q_s = 0, 0.5\ 1, \ldots$. The last quantities are directly observed and noted, the interfringe spacings are measured, and the wavelengths are read from the calibration plot $b(\lambda)$ performed earlier.

The accuracy of fringe coincidences/anticoincidences can be evaluated by analysing the deviations (Δc) of the quantity $c = m_s b_s$ in a specific interferometric situation referred to as object-adapted variable wavelength interferometry in the domain of interfringe spacings and denoted by the acronym AVAWI(b), after [1] and [2]. As long as the conditions of the AVAWI(b) procedure are fulfilled, $c = m_s b_s$ is theoretically a constant quantity. In practice, however, some deviations Δc occur and we take an average quantity C defined as

$$C = \overline{m_s b_s} = \frac{1}{S} \sum_{s=1}^{S} (m_1 + q_s) b_s \tag{8}$$

where S is the overall number of coincident/anticoincident configurations of interference. The standard deviation σ expressed by a formula similar to that given previously in the footnote and attributed to the quantities $c = m_s b_s$ and then divided by $m_a = (m_1 + m_f)/2$ can be qualified as the inaccuracy of fringe coincidences/anticoincidences provided that the interfringe spacings b_s are precisely measured. Consequently, we may write the inaccuracy in question as

$$\Delta b = \frac{\sigma}{m_a} = 2 \frac{\sigma}{m_1 + m_f}, \tag{9}$$

where m_1 and m_f are the values of the first and final fringe coincidences/anticoincidences, respectively ($m_f = m_1 + q_f$). The above expression is quite understood due to the fact that the inaccuracy in question causes the interfringe spacing b to be slightly varied with respect to its true value attributed to the ideal fringe coincidence or anticoincidence. Moreover, Eq. (9) shows that Δb decreases if the initial interference order m_1, hence m_f and m_a increase. Here, as is usual, m_1 is selected in the longwave (red) region of the visible spectrum, and thus m_f and m_a relate to the shortwave (blue) and middle-wave (yellow) spectral regions, respectively.

The above approach permits us to evaluate rather a synthetic (average) accuracy of fringe coincidences/anticoincidences, and can be used if the conditions of the AVAWI(b) procedure are fulfilled, as mentioned earlier. Some results of measurement by using the AVAWI(b)–1 technique have been reported earlier, and the analysis of those results shows that Δb is smaller than 0.5 μm for cylindric objects (fibres) and not higher than 0.1 μm for plate-like objects. For the microinterferometer used, $\Delta b = 0.1$ μm in the interfringe domain is equivalent to $\Delta\lambda = 0.3$ nm in the wavelength domain, and thus a possible inaccuracy $\Delta\delta$ in the determination of the optical path differences $\delta_s = m_s \lambda_s$ of an object under study can be equal to $\Delta\delta = m\Delta\lambda$. In favourable circumstances ($m_1 = 10$ or more, straight-line interference fringes displaced by the object), the relative error $\Delta\delta/\delta$ is as small as 0.01%.

Another approach to the problem under discussion must be made if the technique AVAWI(b)–1 does not hold, and thus the quantities $m_s b_s$ are not constant but they systematically increase or decrease as the light wavelengths λ_s become more and more

short. In such a situation, a representative number (e.g., 10) of a given fringe coincidence/anticoincidence and the interfringe spacing measurement are simply repeated. The standard deviation σ then calculated and expressed in the unit attributed to the interfringe spacing b can be qualified as the error Δb due to the inaccuracy in the fringe coincidence/anticoincidence if the spacing b has been measured in a way extremely precise. Otherwise, Δb inlcudes also a contribution due to the inaccuracy of the interfringe measurement. This approach shows that the errors Δb are slightly higher than 0.5 μm as far as it concerns the assessment of the fringe coincidence/anticoincidence accuracy.

Let us now concider the techniques VAWI–2 and VAWI–3. The latter uses a single pointer line (PL, Fig. 1 or Fig. 4), and the centres of high-order interference fringes displaced by an object under study are brought into coincidence with this line, when the wavelength of the monochromatic light is decreased. Each coincidence operation is followed by the measurement of the interfinge spacing. A possible inaccuracy in the coincidence leads to an error Δb whose values are a little more or less than those attributed previously to the VAWI–1 technique and its AVAWI(b)–1 version (the approach that has been used to this version can also be applied to the VAWI–3 technique if the conditions of object-adapted interferometry in the interfringe domain are fulfilled). For example, Tab. 4 in [2] shows that $\Delta b = \sigma/m_a = 0.12$ μm, and we can generally accept $\Delta b \approx 0.1$ μm if the AVAWI(b)–3 holds. Otherwise, the inaccuracies Δb are higher than 0.5 μm; these are shown in Table 3. Each standard deviation $\sigma(= \Delta b)$ specified in this table is calculated from ten readings the scale of the phase screw (PS, Fig. 1), preceded by repeating adjustments of the centre of

Table 3. Typical inaccuracies ($\sigma = \Delta b$) in adjusting the centre of interference fringes of different orders to the coincidence with the pointer line, expressed in the unit (μm) attributed to the interfringe spacing b

Spectral region	Interference fringe orders		
	±1	±5	±10
blue	0.80	2.30	1.51
	1.49	0.97	1.13
green	0.82	1.08	1.62
	0.63	0.97	1.35
yellow	1.20	1.01	2.00
	0.53	1.29	1.99
red	0.79	1.61	1.37
	0.65	1.13	0.99
mean values:	0.86	1.30	1.50

a given interference fringe to the pointer line. As can be seen, the deviation increases with increasing interference orders (due to the moderately monochromatic light produced by the VERIL S filter, the fringes of higher orders are wider and their contrast is lower). It is also worth noting that the deviations σ in yellow light are

greater than those in the other spectral regions. This difference has been caused by the fact that the monochromacity of the filter used was evidently weaker in its yellow segment.

On the other hand, the VAWI–2 technique uses two pointer lines whose separation is selected to be as large as possible, say, equal to $10b_1$, as mentioned in Section 2. One of these lines enables the centre of the zero-order fringe of the empty interference field to be brought into coincidence with it permanently, while the consecutive high-order fringes, undisplaced of the empty interference field and then displaced by the object under study, are brought into coincidence with the other pointer line when the wavelength of the monochromatic light is decreased. We have now three operations leading to the coincidences mentioned above. A possible inaccuracy of the first one is not important, the second is always performed under the conditions of the object-adapted interferometry in the interfringe spacing domain, thus introduces very small errors to the final results of interferometric measurements, and the third does not differ from that occurring the VAWI–3 technique. In general, however, the VAWI–2 technique is less accurate than VAWI–3.

6. Self-discipline of the VAWI method

It is important to note that the VAWI method functions under specific conditions which enable the final interferometric results to be protected against errors grater than those spcified in Sections 4 and 5. This ability can be qualified as the "self-discipline" or "self-reliance" of the VAWI method and its various versions.

In particular, the initial interference order m_1 calculated from the formula

$$m_1 = q_s \frac{b_s}{b_1 - b_s} \tag{10}$$

where $s = 2, 3, 4, \ldots$ is a very sensitive test for the correct interferometric process if m_1 will be plotted as a function of the interference order increment q_s. A number of such plots are shown in Fig. 5. These are derived from the measuring data reported in [1] dealing with microinterferometry of polymer textile fibres. As can be seen, we can distinguish three situations: i) the function $m_1(q_s)$ goes up, ii) comes down, or iii) remains practically constant with increasing q_s. The first situation occurs when the term

$$N_{s1} D_{1s} > 1 \tag{11}$$

where

$$N_{s1} = \frac{n_s - 1}{n_1 - 1} \tag{12}$$

and

$$D_{1s} = \frac{D_1}{D_s} = \frac{(n_e - n_o)_1}{(n_e - n_o)_s} . \tag{13}$$

Here D is, as previously, the birefringence of the quartz crystal of which the

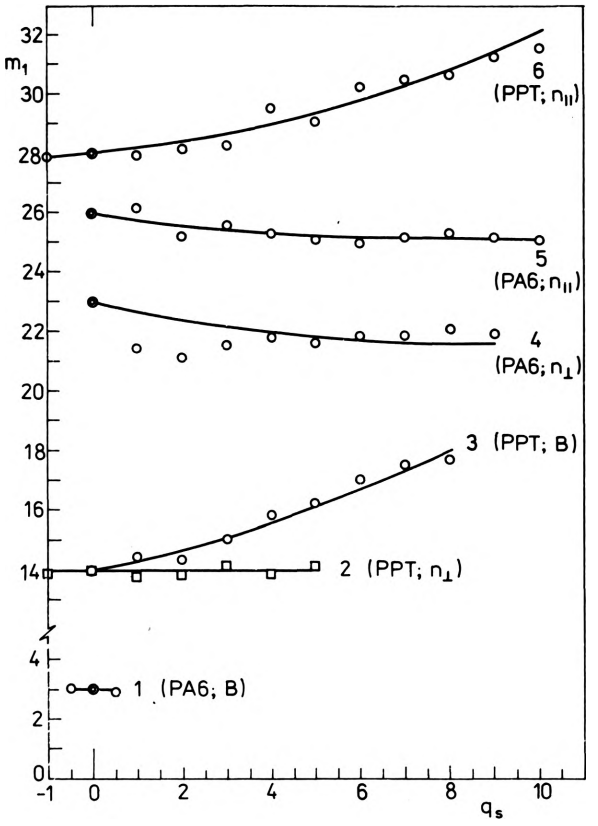

Fig. 5. Plots of the initial interference order m_1 (following directly from Eq. (10)) as a function of the interference order increments q_s arising with decreasing the light wavelength from the red to blue spectral regions. PA6 – polyamide 6 fibre, PPT – poly(p-phenylene terephthalamide) fibre, B – birefringence, $n_{\parallel}$ and $n_{\perp}$ – refractive indices of fibres for polarized light vibrating parallel and at light angles to the fibre axis. Doubly encircled points represent the true initial interference orders. Data after [11]

Wollaston prisms of the microinterferometer in question are made ($D = n_e - n_o$), and n is the refractive index of an object under study surrounded by an air medium and measured in transmitted light. The subscripts 1 and s refer to the wavelengths λ_1 and λ_s. On the other hand, the second situation occurs if

$$N_{s1}D_{1s} < 1. \tag{14}$$

Normally, the coefficient N_{s1} is higher and D_{1s} is smaller than unity; and thus, a specific situation is possible when $N_{s1} = 1/D_{1s}$ or

$$N_{s1}D_{1s} = 1. \tag{15}$$

This situation has been referred to as the object-adapted interferometry in the interfringe domain, AVAWI(*b*), and the function $m_1(q_s)$ takes a constant value. If the birefringence B of a fibre or of another anisotropic object is measured, then the coefficient N_{s1} in expressions (11)–(15) is replaced by $B_{s1} = B_s/B_1$.

The distribution of the experimental points in Fig. 5 is not quite regular due to inevitable errors in the coincident/anticoincitent configurations of interference fringes (see Fig. 3 and 5 in [11]). Nevertheless, the true plot of the function $m_1(q_s)$

is obviously well defined. Some doubts are only produced by the experimental points which constitute the plot $m_1(q_s)$ denoted by No. 4. This can be qualified as a result of an inaccurate measuring process. The dobuts, however, can be dispelled if the products $m_s b_s = (m_1 + q_s)b_s = c_s$ are analysed as a function of q_s (Fig. 6). The initial

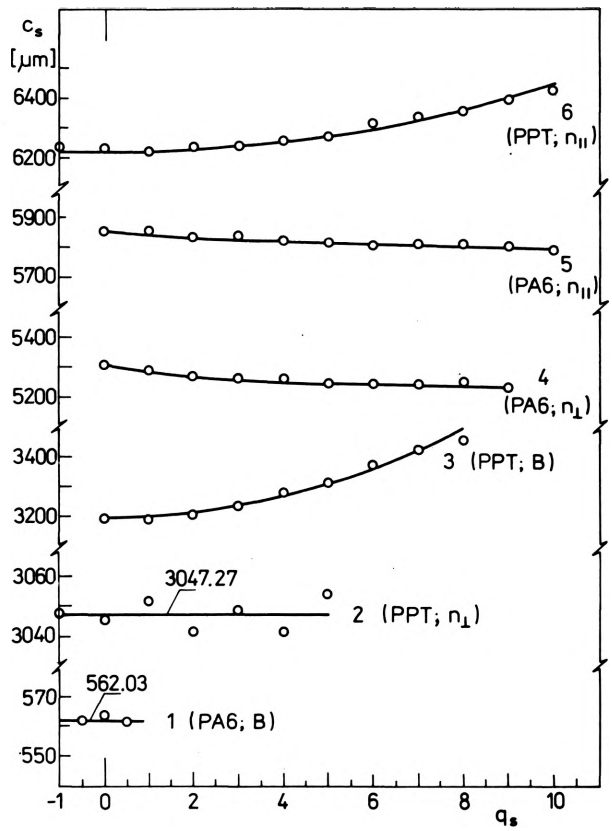

Fig. 6. As Fig. 5, but the plots of $c_s = m_s b_s = (m_1 + q_s)b_s$ as a function of q_s

interference order m_1 is now the true integer order (or an expected true initial order), while previously (Fig. 5) it was given by a series of numbers which resulted from Eq. (10). In general, however, this equation is an approximate formula, and applies strictly only to the AVAWI(*b*) method.

As can readily be seen, the distribution of experimental points is more regular than that in Fig. 5 and the rising and descending or horizontal character of the graphs is clearly seen. Note that the vertical scale of the graphs 3–6 and that of graphs 1 and 2 in Fig. 6 is magnified two and twenty times, respectively, in relation to the vertical scale of the respective graphs in Fig. 5.

Finally, the coefficients:

$$\Lambda_s = \frac{\lambda_s}{n_s - 1}, \tag{16}$$

and

$$\Lambda_s = \frac{\lambda_s}{B_s} \tag{17}$$

can be analysed as a function of the light wavelength if the refractive index n or birefringence B is determined. In general, the functions $\Lambda(\lambda)$ are linear or nearly linear for transparent materials whose spectral dispersions $n(\lambda)$ and $n(B)$ are normal (Fig. 7). Additionally, the tangents

$$T = \frac{\Delta\Lambda}{\Delta\lambda} \tag{18}$$

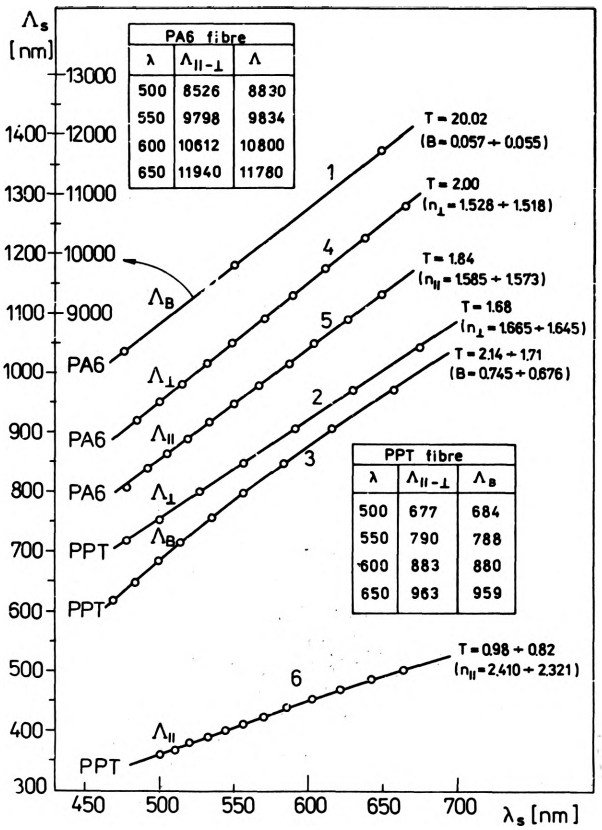

Fig. 7. As Figs. 5 and 6, but the plots of $\Lambda_s = \lambda_s/(n_s - 1)$ as a function of light wavelengths λ_s. T – tangent is defined as $\Delta\Lambda/\Delta\lambda$

can be calculated along the wavelength spectrum. These should be constant within the visible spectrum or only slightly decreasing from the violet to red spectral regions. Otherwise, if the function $T(\lambda)$ increases with the increasing light wavelength λ, the measuring process is certainly not free from some errors.

The birefringence B of a polymer fibre or any other anisotropic object can be measured directly or derived from the refractive index measurements as the

difference $n_{\parallel}-n_{\perp}$. If the quantity Λ_B refers to the first situation and $\Lambda_{\parallel-\perp}$ to the latter, then $\Lambda_{\parallel-\perp}$ should of course be equal to Λ_B. In practice, however, some discrepancies can occur. These specified in Fig. 7 are tolerable. From the plots $\Lambda_{\parallel}(\lambda)$ and $\Lambda_{\perp}(\lambda)$ it follows that

$$\Lambda_{\parallel-\perp} = \frac{\Lambda_{\parallel}\Lambda_{\perp}}{\Lambda_{\perp}-\Lambda_{\parallel}}. \tag{18}$$

The accuracy analysis described above is a time-consuming operation. If, however, a personal microcomputer is used the analysis is quite trivial and leads fastly to the final results.

7. Quasi-adaptive procedure

It has been experimentally verified that the AVAWI(*b*)–1 and AVAWI(*b*)–3 techniques enable the measuring accuracy to be improved by two orders of magnitude compared with that of conventional techniques of two-beam interferometry. Object-adapted interferometry, however, occurs only in some specific situations. In practice, the most typical interferometric situations are those which can be qualified as the quasi-object-adapted ones (QA) where the term $N_{s1}D_{1s}$ (or $B_{s1}D_{1s}$) is only slightly higher or lower than unity. On a limited scale we can therefore use the procedure of object-adapted variable-wavelength interferometry to the QA interferometry.

First of all, the same formula (10) is used for calculating the initial interference order m_1. Sometimes, the formula

$$m_1 = q_s \frac{\lambda_s}{\lambda_1-\lambda_s} \tag{19}$$

may also be useful for finding m_1. In general, the approximate value for m_1 calculated from Eq. (19) will be slightly greater than the true value due to the fact that the coefficient N_{s1} is always slightly higher than unity if the spectral dispersion $n(\lambda)$ is normal. For instance, if Eq. (19) gives $m_1 = 13.2$ in the red and/or orange region of the spectrum, the true initial interference order m_1 may be, at most, equal to 13. On the order hand, the approximate value for m_1 calculated from Eq. (10) will be slightly greater or smaller than, or equal, to the true integer value due to the fact that the coefficient D_{1s} is always slightly lower than unity, and thus the term $N_{s1}D_{1s}$ can be greater or smaller than, or equal to, unity (see Eqs. (11), (14) and (15)). Moreover, the approximate value for m_1 calculated from Eq. (10) is always smaller than that calculated from Eq. (19).

The above discussion shows that there are sufficient error preventions, as far as it concerns the selection of true integer value for m_1 in the situation of the quasi-object-adapted variable-wavelength interferometry, where the term $N_{s1}D_{1s}$ (or $B_{s1}D_{1s}$) is only slightly higher or lower than unity. Finally, in order to check that the

initial interference order m_1 has been correctly fixed, the coefficient N_{FC}, defined by the relation

$$N_{FC} = \frac{n_F - 1}{n_C - 1}, \tag{20}$$

can also be analysed. Here the subscripts F and C denote the spectral lines of light wavelengths $\lambda_F = 486.1$ nm and $\lambda_C = 656.3$ nm. A wrong initial interference order m_1, differing from the true value by at least unity ($+1$ or -1), leads to a value of the coefficient N_{FC} differing greatly from that characterizing known materials (liquids, polymers, glasses, etc.), whose representative groups are shown in Fig. 8. If the birefringence B is measured, Eq. (20) takes the form $B_{FC} = B_F/B_C$. This coefficient functions in the same way as N_{FC}.

However, the verification of the initial interference order m_1 based on the analysis of the coefficient N_{FC} is limited to the transparent objects whose thickness t is not too great, say, smaller than 20 μm. To prove this statement, we can write the basic equations of the VAWI method in the following form:

$$(n_C - 1)t = m_C \lambda_C, \tag{21a}$$

$$(n_F - 1)t = (m_C + q_F)\lambda_F \tag{21b}$$

where the initial interference order $m_1 = m_C$ is "coincident" with the light wavelength λ_C and the interference order increment q_F corresponds with the wavelength λ_F. Such a situation is achieved if the object thickness

$$t = m_C \frac{\lambda_C}{n_C - 1}, \tag{22}$$

thus

$$m_C + q_F = t \frac{n_F - 1}{\lambda_F} \tag{23}$$

and

$$N_{FC} = \frac{\lambda_F}{\lambda_C} \frac{m_C + q_F}{m_C} = 0.7407 \frac{m_C + q_F}{m_C}. \tag{24}$$

The above formulae follow directly from Eqs. (21).

Now we can arbitrarily select a transparent object and suppose a series of initial interference orders n_C to be equal, say, to 5, 10, 15,.... For each n_C we calculate from Eqs. (22)–(24) the thickness t, the interference order $m_C + q_F$, and the coefficient N_{FC}. Then we take $m_C + 1$ and $m_C + q_F + 1$, then $m_C - 1$ and $m_C + q_F - 1$ and calculate, respectively, the coefficients $N_{FC}(+1)$ and $N_{FC}(-1)$ for which the initial interference order m_C, and consequently also $m_C + q_F$ are increased and decreased by unity. Finally, we take differences

$$\Delta N_{FC}(+1) = N_{FC}(+1) - N_{FC}, \tag{25a}$$

$$\Delta N_{FC}(-1) = N_{FC}(-1) - N_{FC}. \tag{25b}$$

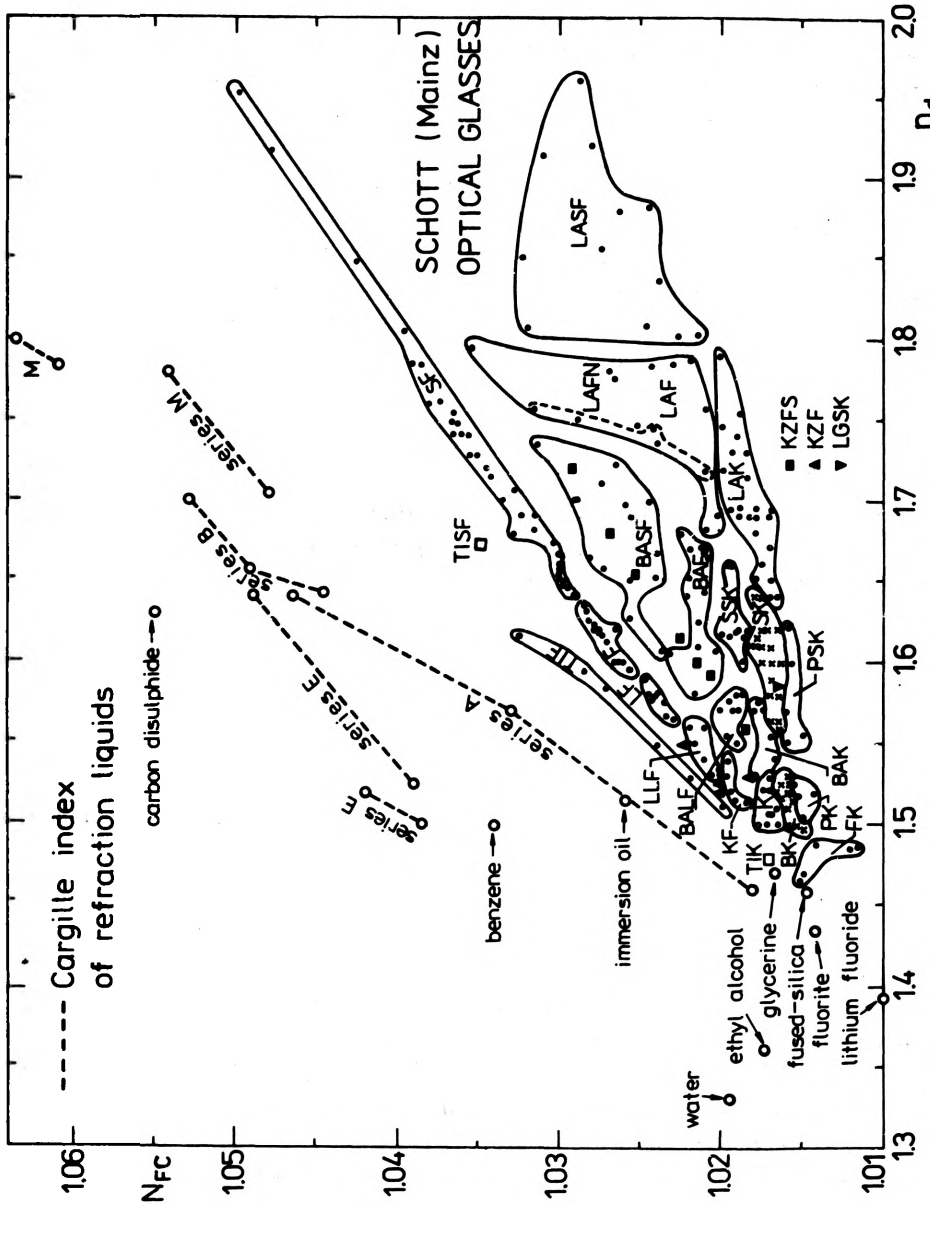

Fig. 8. Optical glasses (Schott, Mainz) and refraction liquids (Cargille), and some other liquid and solid substances respented diagramatically by their dispersion coefficient $N_{FC} = (n_F - 1)/(n_C - 1)$ plotted as a function of refractive index n_d (or n_D)

Table 4 and Fig. 9 show that these differences become smaller and smaller as the object thickness t, and thus the initial interference order m_C increase. For $m_C = 30$, the differences $\Delta N_{FC}(+1)$ and $\Delta N_{FC}(-1)$ are quite small and cannot be qualified as an authoritative test for verifying the true value of the initial interference order.

Table 4. Exemplary data for illustrating Eqs. (22)–(25) and the following text, Fig. 9, and Eq. (28)

	$n_D = 1.5800$		$n_C = 1.5729$			$n_F = 1.5983$	
m_C	t [μm]	$m_C + q_F$	Number of fringe coincidences S_{fc} between λ_C and λ_F	$m_C + 1$	$m_C - 1$	N_{FC}	$\Delta N_{FC}(\pm 1)$
5	5.7279	7.05	3	–	–	1.0443	–
				6	–	0.9937	−0.0506
				–	4	1.1200	0.0757
10	11.4558	14.10	5	–	–	1.0443	–
				11	–	1.0167	−0.0276
				–	9	1.0781	0.0338
15	17.1836	21.1496	7	–	–	1.0443	–
				16	–	1.0253	−0.0190
				–	14	1.0660	0.0217
20	22.9115	28.1999	9	–	–	1.0443	–
				21	–	1.0299	−0.0144
				–	19	1.0603	0.0160
30	34.3673	42.2998	13	–	–	1.0443	–
				31	–	1.0345	−0.0098
				–	29	1.0548	0.0105

Moreover, it is important to note that $\Delta N_{FC}(+1)$ and $\Delta N_{FC}(-1)$ only slightly depend on the refractive index of an object under study, as shown in Fig. 9 (the plots for $n_D = 1.33$ and $n_D = 1.80$ run close to each other).

Another important operation in the QAVAWI procedure is the refinement of the directly measured quantities, i.e., the interfringe spacings b_s. Consequently, we calculate the products $m_s b_s = c_s$ and produce the plot of c_s as a function of q_s, such as shown in Fig. 6 (see graphs 3–6). From the regular line, which averages the experimental points we read $\tilde{c}_s$ and then calculate $\tilde{b}_s = \tilde{c}_s / m_s$. The interfringe spacings $\tilde{b}_s$ are slightly greater or smaller than and sometimes equal to b_s, but generally more accurate than b_s due to the fact that this averaging operation diminishes inevitable defects in fringe coincidences/anticoincidences discussed earlier. For the final interferometric results, the wavelength values λ_s are required. These are read from the calibration plot $b(\lambda)$ for $\tilde{b}_s$.

Due to the procedure proposed above the QAVAWI–1 and QAVAWI–3 techniques enable the measuring accuracy to be improved by at least an order of magnitude compared with that of conventional methods of two-beam interferometry.

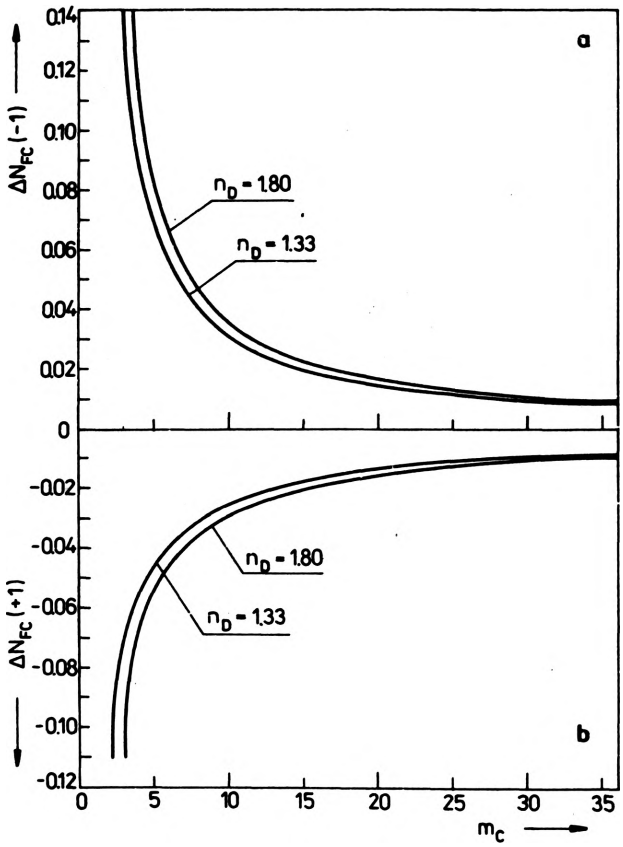

Fig. 9. Plots of Eqs. (25) as a function of the interference order m_C for transparent object such as optical glasses or refraction liquids of different refractive index n_D (from 1.33 to 1.80)

8. Number of fringe coincidences within the spectral region $\lambda_C - \lambda_F$

From Equations (22) and (23) it follows that the interference order increment

$$q_F = m_C\left(\frac{\lambda_C}{\lambda_F}\frac{n_F-1}{n_C-1} - 1\right) = m_C(1.35N_{FC}-1). \tag{26}$$

The coefficient N_{FC} ranges practically from 1.015 to 1.05 (see Fig. 8), and thus

$$q_F \approx 0.4m_C. \tag{27}$$

The number of fringe coincidences (S_{fc}) whithin the spectral region between the wavelengths λ_C and λ_F (including these wavelengths) is given by

$$S_{fc} = q_F + 1 = 0.4m_C + 1 \tag{28}$$

where $q_F = 0.4m_C$ is taken an integer number the nearest to but smaller than

the value following from Eq. (27). If, for example, $m_C = 2$, the increment $q_F = 0.8$ and $S_{fc} = 1$ (the fringe coincidence occurs only for λ_C, practically in the red spectral region). If, however, $m_C = 3$, the increment $q_F = 1.2$ and $S_{fc} = 2$; similarly, for $m_C = 4$, 5, 6,..., we have $q_F = 1.6$, 2, 2.4,..., and $S_{fc} = 2$, 3, 3,..., respectively.

In order to use effectively the VAWI–1 and VAWI–3 techniques, we require at least one fringe coincidence and two fringe anticoincidences (see graph 1 in Figs. 5–7) or two coincidences and one anticoincidence between them. For $m_C = 1$ we have only one coincidence, for $m_C = 2$ also one coincidence and one anticoincidence ($q_F = 0.8$, but the first anticoincidence requires $q = 0.5$). Consequently, the VAWI–1 and VAWI–3 techniques can start if the initial interference order m_C (in general, m_1 in the longwave region of the visible spectrum) is equal to 3. This is just the case of graph 1 in Figs. 5–7.

On the other hand, the maximum number for m_C (or m_1) is theoretically unlimited. In practice, however, the limit is determined by three factors: i) the degree of light monochromacity, ii) the spectral resolution of the increments q_s if m_C is very high, say, $m_C > 500$ or $q_F > 200$, iii) the correct determination of the initial interference order m_1 from Eqs. (10) and/or (19) when m_1 is very high and the object-adapted interferometry, AVAWI(b) or AVAWI(λ), does not hold. Among these factors the most critical is the first one as far as the wedge interference filter Veril S is used. The maximum number for m_C (or m_1) cannot be recommended with this filter the greater than 40 or maximally 50. Thus, the range of optical path differences suitable for the measurement using the VAWI–1 and VAWI–3 techniques lies between $3\lambda_C$ and $40\lambda_C$ (maximally $50\lambda_C$). On the other hand, the optical path differences smaller than $3\lambda_C$ (or even smaller than $5\lambda_C$) can be measured using the VAWI–2 technique (see [7] and [8]).

9. Reflected-light VAWI method

The accuracy problems of the reflected-light VAWI method are the same as those of the transmitted-light VAWI method discussed in the preceding sections. It is, however, worth noting that in reflected light the object-adapted interferometry in the wavelength domain occurs if an object under study (O, see Fig. 1 in [9]) and its substrate (S) are surrounded by an air medium and do not produce a phase jump ($\Delta\psi = 0$). In such a situation, the basic equations of the VAWI method have the forms:

$$\delta_1 = 2t = m_1\lambda_1, \tag{29a}$$

$$\delta_s = 2t = (m_1 + q_s)\lambda_s \tag{29b}$$

where t is the object height (or the depth of a groove). From these equations it follows formula (19), which signifies that the AVAWI(λ) occurs. Its accuracy is the same as or similar to that of the AVAWI(b) method discussed earlier.

By analogy with Equations (21), the above equations may be rewritten as:

$$2t = m_C\lambda_C, \tag{30a}$$

$$2t = (m_C + q_F)\lambda_F, \tag{30b}$$

and we obtain

$$q_F = m_C\left(\frac{\lambda_C}{\lambda_F} - 1\right) = 0.35m_C, \tag{31}$$

and

$$S_{fc} = 0.35m_C + 1. \tag{32}$$

Consequently, the number of fringe coincidence (S_{fc}) within the spectral region between the wavelengths λ_C and λ_F is nearly the same as that in transmitted-light interferometry (compare Eqs. (27) and (28)).

Usually, we arrange experiments to fulfil the conditions of the AVAWI(λ) method in reflected light; and thus, a further discussion of the reflected-light interferometry appears to be useless. In general, the AVAWI(b) method is more powerful than AVAWI(λ). The former, however, does not work in reflected light (except gradient objects; see Sect. 10) when the object under study is surrounded by an air medium and the double-refracting interference system in question is used (see [2]). It is also worth noting that the achromatic thickness t_a (height, depth) is about four times smaller in reflected light than that in transmitted light (see Sect. 5 in [9]).

10. VAWI method applied to gradient objects

So far we have confined ourselves to plate-like or cylindrical objects for the sake of their majority in practice, but there are also in special use some prism-like objects, say, such as shown in Fig. 10**a**. This is a refractometric glass plate which, together with an auxiliary plate AP (Fig. 10**b**), constitutes a semi-trapezial channel for a measured liquid L enclosed between a microscope (glass) slide GS

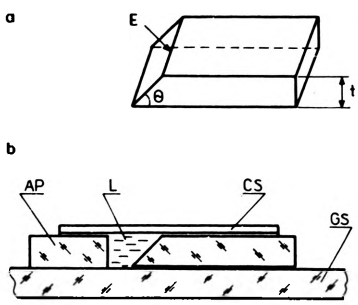

Fig. 10. Prism-shaped glass plate (**a**) and its use for gradient interference refractomerty (**b**)

and a cover slip CS. Such a micro-chamber belongs to the additional equipment of the Biolar PI microinterferometer. Normally, the objective PI 10× is used, whose birefringent prism W_0 (Fig. 1) is crossed with the tube birefringent prism W_2 No. 2, and the micro-chamber (Fig. 10) is placed so that the edge E of its prismatic plate is in focus and oriented at right angles to the interference fringes observed in the image plane of the microinterferometer. The duplicated images E_1 and E_2 of the edge

E divide the field of view into two halves (Fig. 11). One half contains the undisplaced fringes I and the other is occupied by fringes I' displaced by the prismatic part of the refractrometric plate. Both families of fringes are connected by intermediate

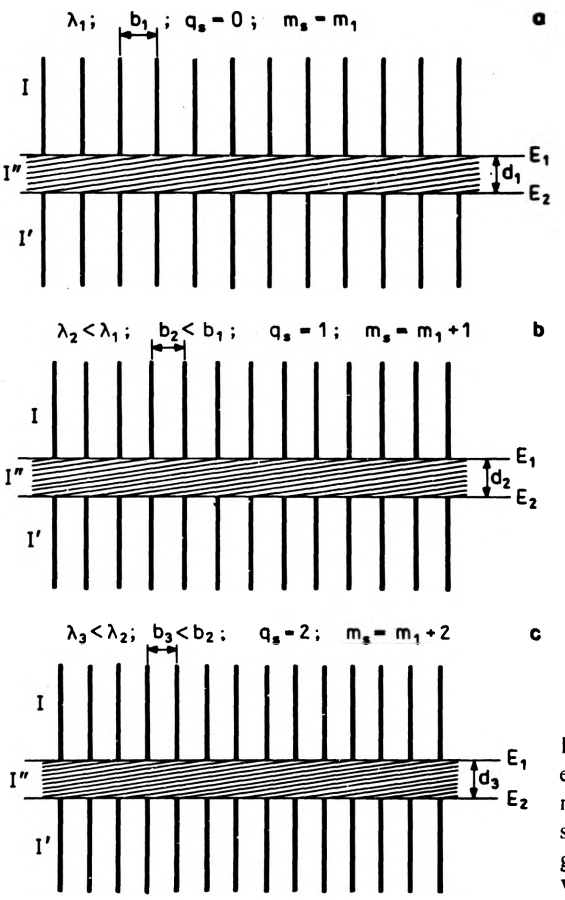

Fig. 11. Coincident configurations of interference fringes I and I' when the double-refracting microinterferometer (Fig. 1) and a prism-shaped glass plate (Fig. 10) are applied to gradient interference refractometry using the VAWI method

interference fringes I' which cross the central part of the field of view between the edge images E_1 and E_2. Thus, no problem arises in identifying the orders of the displaced fringes I' (if the difference between refractive indices n and n' of the prism plate and liquid L is not too large). The displacement of the fringes I' does not express the optical path difference δ in the object plane of the microinterferometer in question, but a gradient of δ in the direction of the wavefront shear. Consequently, the prism region of the refractometric plate can be classified as the gradient object with constant slope. Such an object is especially suitable for precise interferometry using the VAWI–1 technique. The procedure is shown in Fig. 11, where the first three coincident configurations of fringes I and I' are presented. These configurations can be supplemented by fringe anticoincidences one of which is shown in Fig. 12.

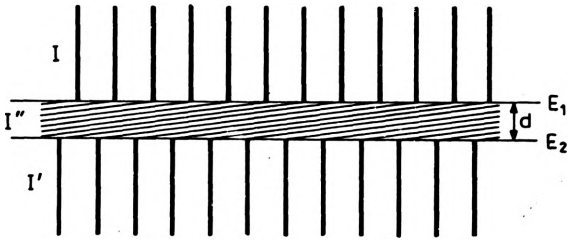

Fig. 12. As Fig. 11, but one of the antico-incident configuration of interference fringes I and I'

Basic equations which apply to the above situation have the following form:

$$\Delta_1 = (n_1' - n_1) d_1 \tan\Theta = m_1 \lambda_1, \tag{33a}$$

$$\Delta_s = (n_s' - n_s) d_s \tan\Theta = (m_1 + q_s)\lambda_s \tag{33b}$$

where Δ_1 and Δ_s are the optical path differences between sheared wavefronts, observed in the image plane of the microinterferometer in question; d_1 and d_s are the wavefront shears in the direction perpendicular to the edge E of the prismatic plate (or parallel to the interference fringes I and I'): and Θ is the apex angle of the prismatic plate as shown in Fig. 10. Note that the wavefront shear d is a function of light wavelength λ and can be expressed as

$$d = \frac{a}{M}\varepsilon = f' 2(n_e - n_o)\tan\alpha_0 = f' 2D\tan\alpha_0 \tag{34}$$

where a is the distance between the back focal point F' and image plane Π', M is the magnifying power and f' is the focal length of the objective Ob, and α_0 is the apex angle of the objective birefringent prism W_0 (Fig. 1).

From Equations (33) it follows that the initial interference order m_1 is given by

$$m_1 = q_s \frac{\lambda_s}{N_{s1}' d_{s1} \lambda_1 - \lambda_s} \tag{35}$$

where

$$N_{s1}' = \frac{n_s' - n_s}{n_1' - n_1}, \tag{36}$$

and

$$d_{s1} = \frac{d_s}{d_1}. \tag{37}$$

If we assume that the focal length f' is free from the spectral dispersion, then Eq. (34) leads to

$$d_{s1} = \frac{D_s}{D_1} = D_{s1}, \tag{38}$$

and by substituting $\lambda = b2B\tan\alpha$ (see Eq. (1)), and (38) into (35), one has

$$m_1 = q_s \frac{b_s}{N'_{s1} D_{s1} D_{1s} b_1 - b_s} . \tag{39}$$

However, $D_{1s} = 1/D_{s1}$, and thus

$$D_{s1} D_{1s} = 1, \tag{40}$$

and we obtain

$$m_1 = q_s \frac{b_s}{N'_{s1} b_1 - b_s} . \tag{41}$$

If $N'_{s1} = 1$, this formula takes the form of Equation (10) and we have the object-adapted interferometry in the interfringe domain. On the other hand, Eq. (35) may also be written as

$$m_1 = q_s \frac{\lambda_s}{N'_{s1} D_{1s} \lambda_1 - \lambda_s} . \tag{42}$$

If $N'_{s1} D_{1s} = 1$, this expression takes the form of Equation (19) and we have the object-adapted interferometry in the wavelength domain.

It will be interesting to compare formulae (41) and (42) with those for non-gradient objects (see Table 1 in [2]). As can readily be seen, the terms N'_{s1} and $N'_{s1} D_{1s}$ are transposed (ε_{1s} in formulae of the table cited above is equal to D_{1s}).

However, a more important fact is expressed by Eq. (40); namely, this equation shows that in gradient interferometry the spectral dispersion of birefringence D of the interference optical system, i.e., $D(\lambda)$, is balanced by the spectral dispersion of wavefront shear d, i.e., by $d(\lambda)$.

In order to determine the refractive index difference $n' - n = \Delta n$, or rather its spectral dispersion $\Delta n(\lambda)$, from Eqs. (33), the spectral dispersion of d, or that of the product $d \tan \Theta$, must, of course, be known. The latter can be determined in different ways. In particular, an additional liquid can be used whose spectral dispersion $n''(\lambda)$ is well known and strongly different from $n(\lambda)$ except for one light wavelength λ_M, referred to as the matching wavelength for which one has $n_M = n''_M$, and thus

$$d_M \tan \Theta = \frac{\Delta_M}{|n'_M - n''_M|} \tag{43}$$

where Δ_M is the respective optical path difference read from the plot $\Delta_s(\lambda)$ prepared previously as a function of light wavelengths λ_s. These wavelengths were read out from the calibration plot $b(\lambda)$ for respective interference spacings b_s which were directly measured in the situation when the first liquid of known refractive index dispersion $n'(\lambda)$ was used. If the term $d \tan \Theta$ is accurately determined for one light wavelength (λ_M) in the above way, then for any other wavelength λ, and especially for λ_s, this term is calculated from the relation

$$d_s \tan \Theta = \frac{\lambda_s}{b_s} \frac{b_M}{\lambda_M} d_M \tan \Theta. \tag{44}$$

Finally, the refractive indices n_s of the prismatic plate can be determined from Eqs. (33), i.e.,

$$n_s = n_s' \pm \frac{\Delta_s}{d_s \tan\Theta} \tag{45}$$

where the sign "+" stands for $n_s > n_s'$ and the sign "−" for $n_s < n_s'$, and the subscript $s = 1, 2, 3, \ldots$. In particular an air medium can be used instead of the first liquid (L, Fig. 10**b**), and thus the refractive index n' may be assumed to be equal to unity over the visible spectrum. This is possible, if the apex angle Θ of the prismatic plate is not too large, say, is smaller than 20°.

If n_s and $d_s \tan\Theta$ are known, the plots of these quantities as a function of λ can be made. These are qualified as the calibration plots of the prismatic plate (once made these plots are permanently valid!), which may then be used for measuring the refractive indices and their spectral dispersions of fluids and liquid-like substances.

The term $d\tan\Theta$ as a function of λ can also be determined in reflected light using the VAWI–1 technique. If the prismatic plate (Fig. 10**a**), whose apex angle Θ is relatively small, say, $\Theta \leqslant 15°$, is illuminated by the microscope objective (Ob, Fig. 1) of the double-refracting microinterferometer in question equipped with an epi-illuminator (see Figs. 3 and 4 in [9]), then we can observe the same interference pattern as that shown in Fig. 11. The basic equations of the VAWI method take now the forms:

$$\Delta_1 = 2d_1 \tan\Theta = m_1\lambda_1, \tag{46a}$$

$$\Delta_s = 2d_s \tan\Theta = (m_1 + q_s)\lambda_s. \tag{46b}$$

From these equations it follows that

$$m_1 = q_s \frac{\lambda_s}{d_{s1}\lambda_1 - \lambda_s} = q_s \frac{\lambda_s}{D_{s1}\lambda_1 - \lambda_s}, \tag{47}$$

or

$$m_1 = q_s \frac{b_s}{D_{s1}D_{1s}b_1 - b_s}, \tag{48}$$

but $D_{s1}D_{1s} = 1$, and Eq. (48) takes the form of formula (10) which shows that the object-adapted interferometry in the interfringe domain holds. Such a situation enables the term $d\tan\Theta$ as a function of λ to be determined more accurately than in transmitted light as described previously.

Here, it is also worth noting that non-gradient objects surrounded by an air medium do not apply to the AVAWI(b) method in reflected light in accordance with formula (49), but they apply to the AVAWI(λ), as can readily be seen from Table 2 in [2].

In refractrometry of liquids and solids the measuring accuracy Δn equal to 0.0001 is normally required. This may be achieved if the term $d\tan\Theta$ is determined with relative error $\Delta(d\tan\Theta)/d\tan\Theta$ not greater than 0.05%. This is quite possible due to

the fact that Δb and then $\Delta\lambda$ as small as 0.05 μm and 0.15 nm can respectively be obtained if the AVAWI(b) method works.

11. Conclusions

The problems discussed in this paper characterize the ability of the VAWI method as far as its measuring accuracy is especially important for the user. Sections 2–8 have delt with transmitted-light interferometry, where transparent objects surrounded by an air medium have been taken into consideration, due to the fact that such objects are not only suitable but also recommended for this of interferometry. The spectral dispersion of refractive index of the air medium is very small in comparison to that of solids or liquids and was therefore ignored.

Section 10 can be qualified as a supplementary material to a number of the previous papers of this series. That section shows that gradient objects behave in another way than the step-like or plate-like objects in wavefront shear interferometry; due to the spectral dispersion of the wavefront shear, the gradient object balances the spectral dispersion of birefringence of the double-refracting interference system.

The repeatability errors mentioned in Section 1 can occur only sporadically since the interference system which has been applied to the VAWI method is normally free from these errors. Only some mechnical defects of the transverse movement of the tube birefringent prism (W_2, Fig. 1) may sometimes be responsible for the errors of this kind. These, however, are easily recognizable and can immediately be removed from the measurement process.

In summary, the VAWI method is much more accurate than conventional techniques of visual two-beam interferometry. In particular, the AVAWI(b)–1 or AVAWI(b)–3 technique enables the measuring accuracy of the optical path difference to be improved by two orders of magnitude, while the QAVAWI procedure offers us the accuracy better by at least an order of magnitude.

The VAWI method is suitable for full automatic or at least semi-automatic photoelectronic operation. However, no further improvement of its measuring accuracy is expected by using, say, a CCD camera coupled with a respective processor and microcomputer. Nevertheless, a computer-aided version of the VAWI method is greatly required due to the time consuming calculations leading to the final interferometric results.

References

[1] PLUTA M., J. Opt. Soc. Am. A**4** (1987), 2107–2115.
[2] PLUTA M., Opt. Appl. **18** (1988), 75–92.
[3] PLUTA M., Opt. Appl. **20** (1990), 259–273.
[4] PLUTA M., J. Microscopy **146** (1985), 41–54.
[5] PLUTA M., Opt. Appl. **16** (1986), 141–157.
[6] PLUTA M., Pomiary Automatyka Kontrola **7** (1961), 183–189 (in Polish).
[7] PLUTA M., Opt. Appl. **16** (1986), 301–323.
[8] PLUTA M., Opt. Appl. **17** (1987), 141–151.

[9] PLUTA M., Opt. Appl. **16** (1986), 159–174.
[10] PLUTA M., Opt. Appl. **12** (1982), 19–36.
[11] PLUTA M., J. Microscopy **149** (1988), 97–115.

Received April 4, 1991

Интерферометрия с непрерывно-переменной длиной волны. IX. Точность

Универсальный интерферометрический метод (VAWI) был разработан и описан в предыдущих работах на эту тему. Метод состоит в применении монохроматического света постоянно переменной (уменьшаемой) длины волны и приведении к будущим в совпадении и/или несовпадении конфигурациям сдвинутых и несдвинутых интерференционных полос (техника VAWI–1). В другом варианте метода VAWI применяются две индикаторные линии, которых взаимное расстояние равно около 10 межполосным расстояниям в красной части видимого спектра (техника VAWI–2). Одна из этих линий постоянно совпадает с центром нулевой полосы порядка пустого интерференционного поля, зато на вторую линию приводятся к совпадении, вместе с изменением длины световой волны, очередные интерференционные полосы высоких порядков, сдвинутые исследуемым предметом. В промежуточном варианте между VAWI–1 и VAWI–2 применяется лишь одна индикаторная линия для совпадения с ней интерференционных полос (техника VAWI–3). Эти техники, их основы и применение были описаны в предыдущих работах на эту тему, с особенным учетом их использования в бирефракционной интерферометрии. В настоящей работе подробно обсуждаются измерительные точности этих техник.

Перевел Станислав Ганцаж